VIBGYOR ePress

International Journal of Nanoparticles and Nanotechnology

ISSN: 2631-5084

Influences of Primary Particle Size, Concentration, Ionic Species, and Aggregation States on Transport Efficiency in Single Particle-Inductively Coupled Plasma-Mass Spectrometry Analysis of Metal-Based Nanoparticles

Wen Zhang[1]* and Ying Yao[2]

[1]*Department of Civil & Environmental Engineering, New Jersey Institute of Technology, USA*

[2]*Meadowlands Environmental Research Institute (MERI), USA*

Abstract

In the determination of sizes and concentrations of nanoparticles (NPs), single particle-inductively coupled plasma-mass spectrometry (SP-ICP-MS) suffers uncertainties in the transport efficiency of nebulized liquid droplets of NPs. Many potential factors such as primary particle sizes, concentrations, and ionic components of metal NPs could influence transport efficiency and accuracy of the SP-ICP-MS analysis. This study evaluated the apparent transport efficiency (ε) with six types of metal NPs with sizes of 25-120 nm and concentrations of approximately 10-70 μg/L. Results show that the ε values of hematite NPs remained constant (ε = 0.70 ± 0.15) and did not significantly vary with the primary particle sizes and concentrations. However, the presence of dissolved ferric ions reduced ε, which is consistent with earlier reports. ε values were also shown to vary significantly with the types of metal NPs. More importantly, a higher degree of aggregation or polydispersion caused an evident reduction of transport efficiencies. The monodisperse suspensions of CeO_2 and Ag NPs led to high ε values around 0.86-0.97, suggesting that transport efficiency (e.g., nebulization) could be greater for monodisperse NP suspension than for polydisperse one. The results of this study provided a better understanding of the application principles of SP-ICP-MS toward an accurate analysis of engineered NPs in aqueous samples.

Keywords

SP-ICP-MS, Metal concentration, Nanoparticle, Nebulization efficiency, Transport efficiency

Introduction

Nanotechnology is an important part of modern scientific endeavor that shows promise to improve the quality of human society, to resolve energy or environmental issues, and to provide a substantial economic boost to the society. The world markets for nanomaterials, nanoparticles and nano-enabled products are expected to reach $2.6 trillion by 2015 [1]. Metal nanomaterials such as CeO_2, ZnO and TiO_2 are the largest share of manufactured and applied nanomaterials [2]. They have been widely incorporated into commercial products or industrial processes, including paints, fabrics, personal health care products and food products, [3-5] sunscreens [6] antimicrobial agents, [7,8] solar energy conversion [9,10] and photocatalysis for remediation of environmental pollutants [11,12]. The broad applications of these NPs or nanomaterials may lead to negative consequences (e.g., cellular injury, [13,14] cell membrane disruption, [15-17] and genetic damage[18-20].), when NPs enter the environment and interact with biological systems [21-23]. For instance, studies have shown that ZnO NPs disrupted cell membranes and caused cell death for *E. coli* bacteria [24,25]. Metal-based NPs also demonstrated adverse effects on high-order organisms,[26] including zebrafish embryos [27,28] and *Daphnia magna*, [13,29] human lung cells, [30] red blood cells, [31] and gastrointestinal cells [32]. To assess the potential environmental behavior, fate and biological impacts, accurate detection and quantification of NPs in biological and environmental samples are crucial in the determination of the dose-response relationship and exposure levels [33,34].

Concentrations of metal elements in aqueous samples are commonly analyzed by atomic adsorption spectrometry (AAS), inductively coupled plasma-optical emission spectrometry (ICP-OES) and inductively coupled plasma-mass spectrometry (ICP-MS). Hyphenated methods such as asymmetric flow-field flow fractionation coupled with ICP-MS (AsFlFFF-ICP-MS) provide

***Corresponding author:** *Wen Zhang, Department of Civil & Environmental Engineering, New Jersey Institute of Technology, USA, Tel: 197-359-65-520, Fax: 1-973-596-5790, E-mail: wzhang81@njit.edu*

Received: August 09, 2015: **Accepted:** September 09, 2015: **Published:** September 11, 2015

Citation: Zhang W, Yao Y (2015) Influences of Primary Particle Size, Concentration, Ionic Species, and Aggregation States on Transport Efficiency in Single Particle-Inductively Coupled Plasma-Mass Spectrometry Analysis of Metal-Based Nanoparticles. Int J Nanoparticles Nanotech 1:004

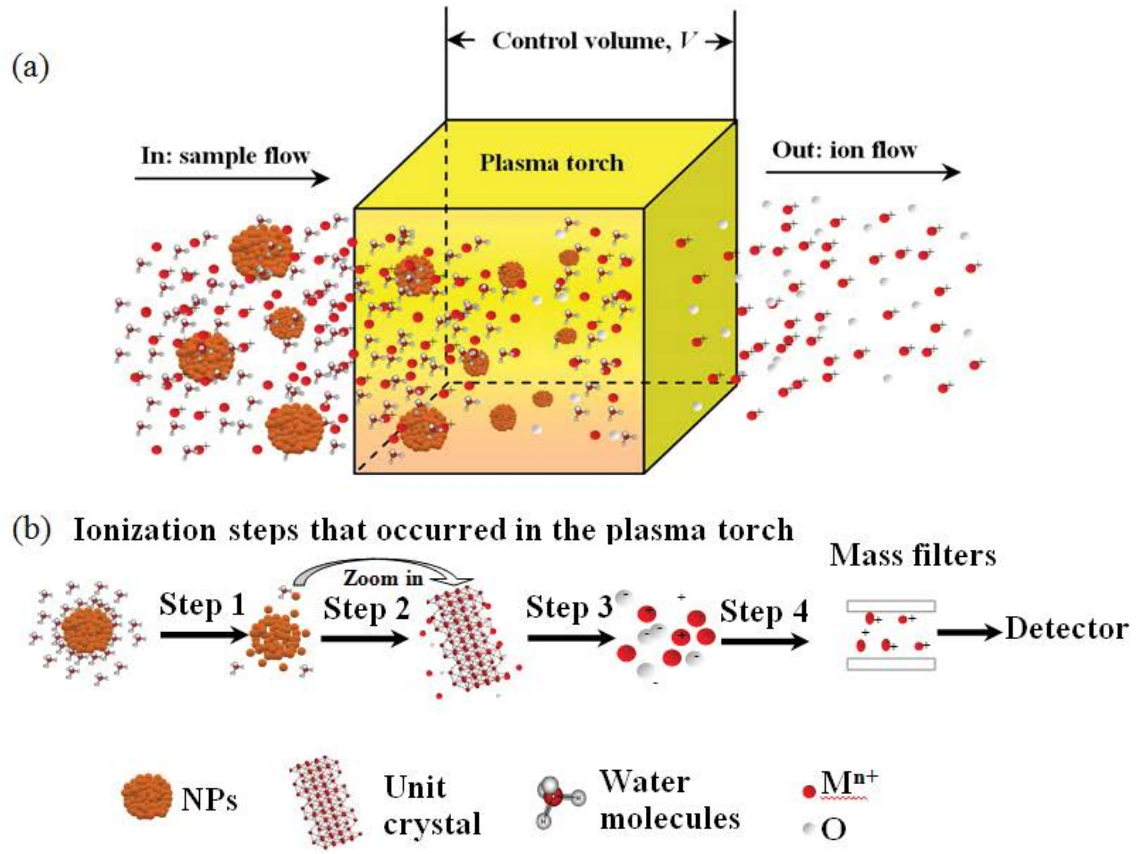

Figure 1: SP-ICP-MS ionization processes of a sample aerosol of metal NPs entering the plasma torch. Step 1: Water molecules are stripped from the surfaces of NPs. Step 2: NPs are decomposed into smaller crystal units. Step 3: NP crystals are decomposed into atoms or ions. Step 4: Electrons are stripped from metal and oxygen atoms (ionization)

additional functionality of separation colloidal particles based on size or charge before measuring metal concentrations by ICP-MS. Single Particle-ICP-MS (SP-ICP-MS), a complementary alternative to hyphenated methods determines particle concentrations within individual particles. SP-ICP-MS does not require separation and thus eliminates potential artifacts from sample preparation. Conventional ICP-MS measures the metal ions dissolved in liquid droplets introduced to the plasma, which ionizes metal ions into plumes for detection. Thus, the signal is constant on the experimental time scale as opposed to episodic signals in SP-ICP-MS, which involves the use of sufficiently diluted suspensions to detect individual NPs. To avoid the measurement of two or more NPs (clusters of NPs), the dwell time must be 1 ms or less (acquisition frequencies of 1000 Hz or higher) [35]. However, low dwell times may increase the risk of measuring a fraction of the whole signal of individual NPs. At present, SP-ICP-MS has intensively been applied to metallic NPs (e.g., Ag or Au) consisting of one element only [35-38]. Characterization of metal oxide or hybrid NPs by SP-ICP-MS is still lacking.

Application of SP-ICP-MS for the determination of the size and number concentration of NPs often suffers insufficient accuracy and uncertainties in the transport efficiency of the particles from the sample introduction system (i.e., nebulizer/spray chamber) to the plasma and the efficiency of the plasma to ablate, atomize, and ionize particulate metals [39,40]. Generally, the plasma can ionize particulates with a similar efficiency to the corresponding dissolved species, [41] because the argon plasma produced by the equipped radio frequency (RF) coil provides high power (up to 1600 W) to rapidly vaporize liquid droplets into gaseous atoms during the sample voyage as shown in Figure 1. However, the transport efficiency of nebulized liquid droplets into the plasma may depend on many factors such as NP types, sizes, aggregation states, concentrations, dissolved metal ions, and surface coating, thereby giving rise to uncertainties in the measurement accuracy. For instance, most researchers have found that particles larger than 2–5 μm may be selectively removed in the spray chamber, [42] which implies that NPs and small aggregates should be more efficiently transmitted to plasma than large colloids or aggregated clusters. Besides the influence of particle size, high solid concentrations or content (0.1–1% w/v) were shown to affect transport efficiency [43,44]. Despite the knowledge about slurry nebulization, there is still a scarcity of information on potential factors (e.g., primary particle size) of the transport efficiency of NPs. This information is clearly important for establishing a complete framework of SP-ICP-MS theories and applications for nanomaterials.

This study evaluated the transport or nebulization efficiency of various commonly used metal NPs (Fe_2O_3, TiO_2, CeO_2, ZnO, Al_2O_3, and Ag NPs) using SP-ICP-MS [45,46]. These metal NPs were selected because they are widely used commercial nanomaterials and have toxicological significance [13,30,32,47-50]. his study examined the influences of primary particle size, particle concentration, and dissolved metal ions on the transport efficiency, which aims to provide fundamental information on the principles of SP-ICP-MS toward a better accuracy control in the analysis of NPs.

Experimental Methods

Chemicals

Table 1 shows the studied NPs and their relevant properties. Different sized hematite NPs were synthesized and thoroughly characterized in our previous studies [32,51-60]. Characterization

Table 1: List of the metal-based NPs used in this study

NPs	Primary Particle Diameters (nm)	Purity (%)	Bulk Density (kg/m³)	Surface coating	Vendor
Hematite (α-Fe_2O_3)	50, 80, 100, and 120	N.A	5300	No coating	Lab-synthesized
TiO_2	25	99.70	4230	No coating	Aldrich
CeO_2	25	99.95	7650	No coating	Aldrich
ZnO	50	99.90	5610	No coating	Aldrich
Al_2O_3	25 40	99.97 99.00	3950	No coating	Nanostructured &AmorphousMaterials
Ag	80	99.00	10500	Citrate	Ted Pella

Table 2: ICP-MS system settings

Parameters	
Nebulizer gas flow	0.91 L/min
Auxiliary gas flow	1.30 L/min
Plasma gas flow	15.25 L/min
ICP RF power	1500 W
Autolense correction	ON
Analog stage voltage	-1525 V
Pulse stage voltage	750 V
Sweeps/readings	25
Replicates	3
Readings/replicate	1

results of other NPs were also reported elsewhere [54,60]. Suspensions of NPs subject to SP-ICP-MS were prepared to be approximately 10-70 μg/L by diluting their stock suspensions with deionized (DI) water. The selected mass concentrations would likely present the number concentration of 10^9-10^{11} L^{-1}, which is greater than the reported detection limits (10^5-10^6 L^{-1}) for NPs by SP-ICP-MS [36,39]. In addition, the selected concentrations of NPs were close to or at comparable orders of magnitude with their environmentally relevant concentrations as predicted previously [53,61]. After dispersal in DI water, the NP suspension was sonicated for 30 min (Misonix sonicator S-4000, Qsonica, LLC) immediately before the SP-ICP-MS analysis. The particle size distribution (PSD) in water suspension was analyzed with the dynamic light scattering (DLS) technique on a Malvern Instruments Zetasizer Nano ZS instrument.

SP-ICP-MS analysis

A PerkinElmer NexION® 300Q ICP-MS was used for data acquisition in the single particle mode. All concentrations were determined from triplicate samples. Error bars represent standard deviations determined from the triplicate measurements. or each measurement, 99000 data points were collected over 50 s using a dwell time of 0.5 ms and a negligible settling time (in the software, data were sent in packages of 1000 data points). The instrument parameters given in Table 2 were optimized using the Elan smart tuning solution (See details in the supplementary file).

Transport efficiencies for different sized hematite nps and different nps: Hematite NPs of different sizes were used as model NPs to evaluate the particle size and concentration impacts on transport efficiency. Our previous work has found no significant dissolution of hematite NPs in water [17]. However, to further eliminate any ionic forms of irons in the NP suspensions, the suspension underwent repeated centrifugation (10000×*g*) and DI water rinsing using Amicon centrifugal ultrafilter with a nominal particle size exclusion of 1-2 nm, which effectively separated all ionic iron forms from hematite NPs. The collected hematite NPs were dispersed in water and used for the following studies. First, regular ICP-MS analysis was performed with complete digestion of the NP suspension to determine the total ferric concentration [M^{n+}]. In the SP-ICP-MS analysis, the concentration of NPs [M^{NPs}] was determined with the same nebulization settings. The apparent mass-based transport efficiency, ε, could be estimated by:

$$[M^{NPs}] = \varepsilon \cdot [M^{n+}] \quad (1)$$

Raw pulse intensity data for NPs were directly compared to the calibration curves of dissolved ionic species to determine the concentrations of NPs, [M^{NPs}]. Eq. (1) was used to experimentally determine values of ε for different sized hematite NPs and other NPs (TiO_2, CeO_2, ZnO, Al_2O_3, and Ag).

The influence of free metal ions ($[M^{n+}]_{free}$) on the transport efficiency: To examine how the presence of dissolved metal ions affects the ionization efficiency of NPs in SP-ICP-MS, ferric ions were spiked into the hematite NP suspensions to reach different dissolved ferric ion concentrations ranging from 5, 10, 20, 35, 50, 75, to 100 μg/L. Two initial mass concentrations of hematite NPs, 13 and 30 μg-Fe/L, were used. The mixed suspension was analyzed by SP-ICP-MS and ε was determined for each case following the same procedure as mentioned in section 4.2.1.

Sample digestion

Sample digestion followed the previous literature [49,62]. Briefly, 1 ml of NP suspension of 10-70 μg/L was digested by adding 2 ml trace level purity HNO_3 (67-70%, w/w) and well mixed on a hotplate at 150°C for 20-30 min. A fully clear and transparent solution indicated the complete sample digestion. Otherwise, 2 ml HNO_3 was added again to the mixture to resume the digestion. Then, the digested solutions were diluted to 10 ml with DI water and stored in 15-ml polystyrene centrifuge tubes (Evergreen Scientfic, USA) until SP-ICP-MS analysis. All glassware and digestion vessels were carefully cleaned and soaked in 10% (v/v) HNO_3 for more than 24 h and finally rinsed five times with DI water prior to use. The concentration of each metal-based NPs was expressed as the concentrations of its ions [M^{n+}].

Statistical analysis

All SP-ICP-MS experiments were carried out triplicate for each condition. The presented results are mean values ± standard deviation from three independent experiments. The differences between experimental groups and control groups were tested for significance using one-way analysis of variance (ANOVA) at a significant level (p = 0.05).

Results and Discussion

The effects of the concentrations and sizes of NPs on the transport efficiency

Figure 2a shows the result comparison for different sized (50, 80, 100, and 120 nm) hematite NPs with three initial mass concentrations (approximately 13, 30, and 60 μg-Fe/L). Compared to the total ferric ion concentrations obtained by the regular ICP-MS analysis on the fully digested samples, the SP-ICP-MS led to lower concentrations of the same hematite NP samples probably due to the lower transport efficiency of NPs compared to dissolved ions. The results of ε presented in Figure 2b did not show strong dependence on particle sizes or the initial concentrations. However, the higher initial mass concentrations seem to slightly increase the transport efficiency. Clearly, the SP-ICP-MS exhibited a quasi-stable efficiency of nebulization, vaporization, atomization, and ionization at 0.70 ± 0.15 for the different sizes and concentrations (10-60 μg/L) for hematite NPs.

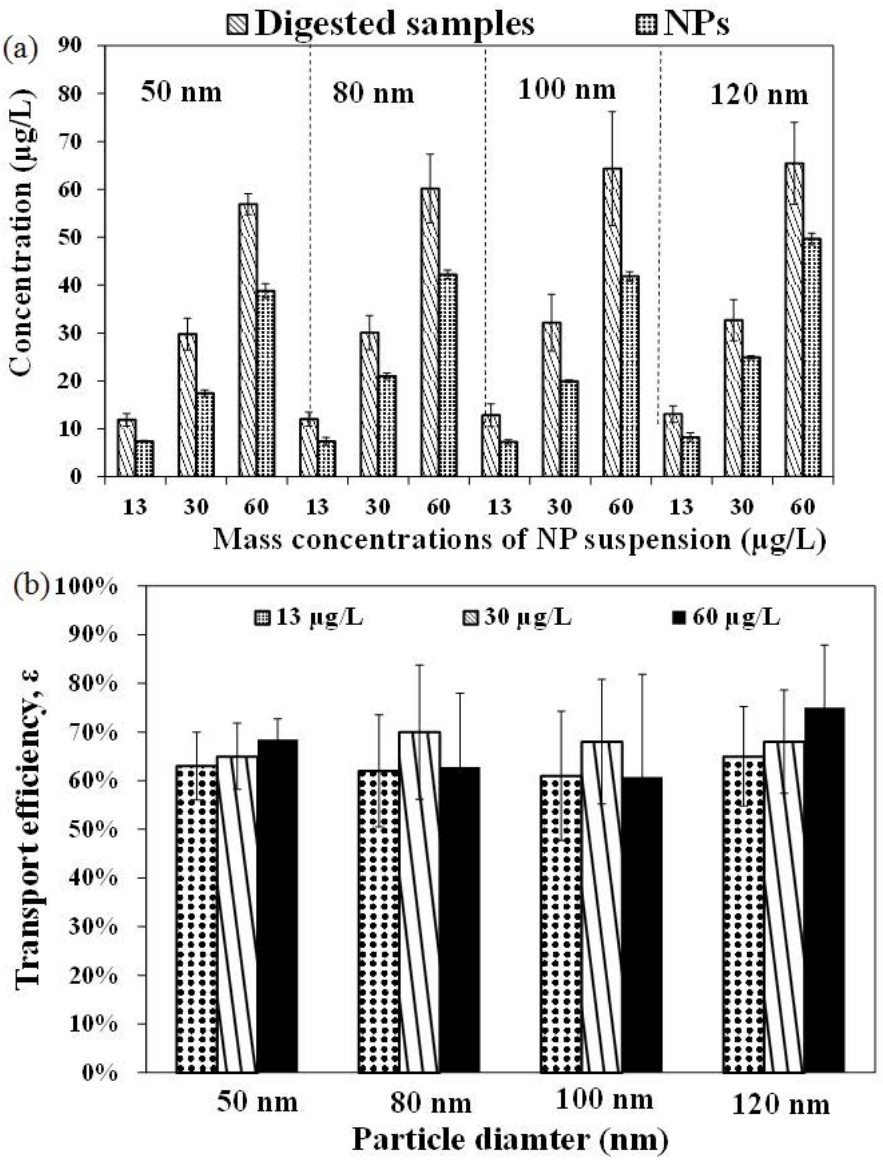

Figure 2: (a) Comparison of the measured concentrations of hematite NPs through regular ICP-MS and SP-ICP-MS. (b) Effects of concentrations and sizes of hematite NPs on the overall efficiency of vaporization, atomization, and ionization.

The influence of free metal ions on the transport efficiency

Figure 3 shows the transport efficiency results of hematite NPs in the presence of different spiked ferric ion concentrations. As the spiked ferric ion concentration increased, the transport efficiency almost linearly decreased (R^2 = 0.92-0.99). After the dissolved ferric ion concentration reached 100 µg/L, the ICP signal was nearly saturated by the dissolved ferric ions, which suppressed the signal counts from NPs. Similar results were reported that dissolved ionic species of silver NPs led to an increase of the signal baseline, probably due to the favorable detection of ICP-MS toward dissolved ionic species other than NPs [37]. These results suggested that in SP-ICP-MS analysis, the ionic components should be eliminated to achieve accurate measurements of individual NPs.

Determination and comparison of transport efficiencies of metal NPs

Besides hematite NPs, other metal NPs we tested also shows similar patterns of the effects from primary particle size, concentration, and ionic species on transport efficiencies (results not shown here). Transport efficiencies varied significantly with the types of NPs, probably due to the differences in particle sizes (hydrodynamic sizes), particle characteristics such as morphology and surface coating or adhesiveness to surfaces of tubing or nebulizer chamber, dispersion or aggregation states. Table S2 shows the hydrodynamic diameters, polydispersivity index (PDI) of different NPs in the water suspension, and the corresponding transport efficiencies. The particle diameters of NPs in Table 1 were determined by TEM or SEM in the solid state of NPs. However, the dispersed NPs may undergo aggregation or hydration that tends to increase the aqueous particle sizes or hydrodynamic diameters determined by DLS. PDI characterizes the degree of dispersion with a value of less than 0.25 indicative of a monodisperse suspension whereas a value greater than 0.25 indicative a polydisperse suspension due to aggregation. Figure 4 shows that transport efficiency likely correlated with hydrodynamic diameters and polydispersivity. A greater hydrodynamic sizes or a greater degree of polydispersivity corresponded to a low level of transport efficiency. For example, two primary particle sizes (25 and 40 nm) of Al_2O_3 were tested and their mean hydrodynamic sizes were 853 and 251 nm respectively. The transport efficiency of Al_2O_3 appeared to decrease with the increase of hydrodynamic diameters, which occurred to other metal NPs as well. This indicates

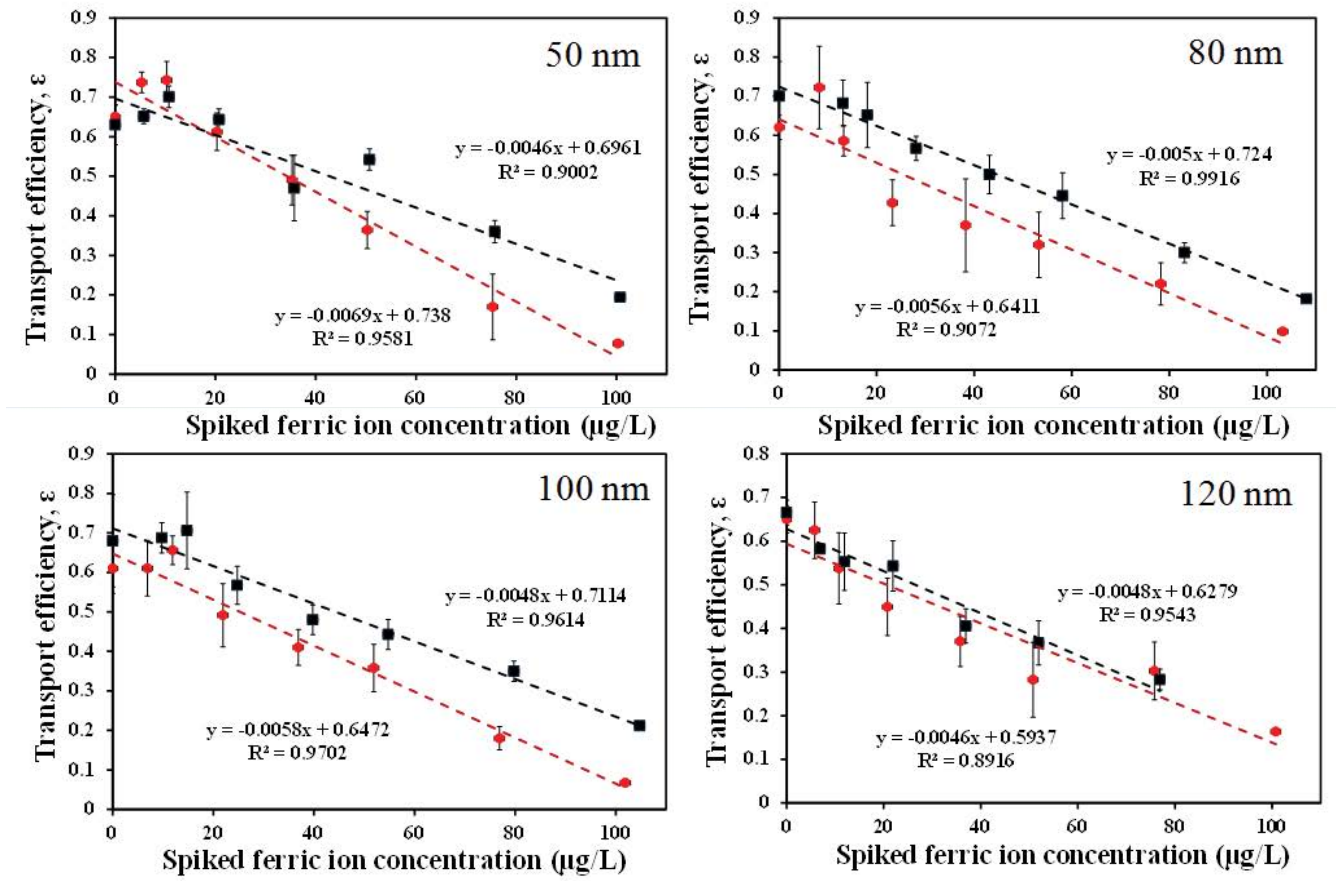

Figure 3: Transport efficiencies of hematite NPs in the SP-ICP-MS analysis with addition of spiked ferric ions at different concentrations shown as the x axis. Hematite NPs were at two initial mass concentrations of 13 µg-Fe/L (●) and 30 µg-Fe/L (■) prior to ferric ion addition. The dashed lines are linear fits for the data with fitting equations shown next to the lines.

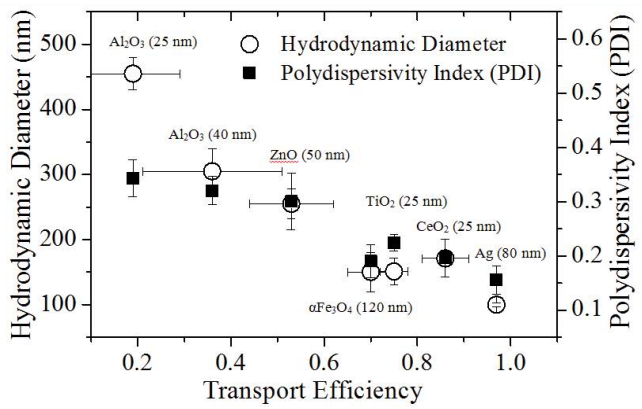

Figure 4: Transport efficiencies of different metal NPs in water dispersion. The primary particle sizes for each type of NPs are given in the parenthesis.

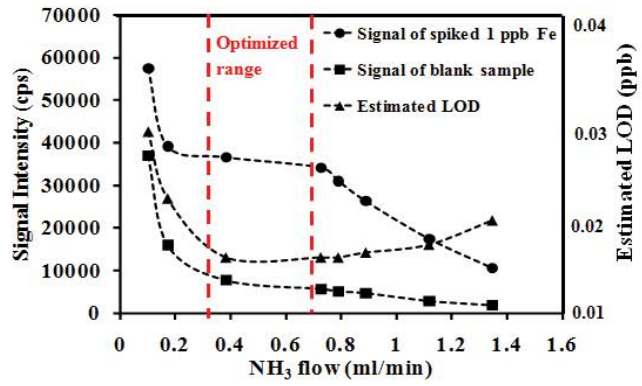

Figure S1. A reduction of noise signal by four orders of magnitude in blank samples (DI water) is achievable with DRC mode, and the detection limit of ^{56}Fe can reach less than 20 ppt.

that aggregated NPs are more likely to be removed in the spray chamber during the transport [42]. Unlike other metal NPs, Al_2O_3 nanomaterials are amorphous and could form hydrolyzed clusters that are sticky or viscous, making it difficult to be nebulized and carried with the moisture vapor. Conversely, a highly monodisperse suspension would likely deliver NPs into the plasma torch in a more efficient way such as Ag NPs, Au NPs, [38] and hematite NPs. Our previous studies show that hematite NPs had excellent stability and monodisperse suspension with hydrodynamic sizes almost consistent with their solid-state particle sizes as determined by TEM or SEM (see results in our previous studies [32,39]). Thus, there was no significant dependence of transport efficiency on particle sizes (the primary solid-state particle sizes) if NPs were monodisperse in water with hydrodynamic sizes around or less than 100 nm. Significant aggregation may potentially reduce the transport efficiency of NPs during the nebulization and voyage into the plasma.

There are many potential factors affecting hydrodynamic size distribution and colloidal stability, such as surface coating or surface adhesiveness to the tubing surfaces. Except Ag NPs, all other metal oxide NPs had no surface coating. Homogenous surface coating could help NPs disperse in liquid suspension, which could improve

Table S1: Analytical methods for each metal element in ICP-MS

Element	Mode	Mass value	Internal standard	Cell gas (mL/min)	Rejection parameter q	Detection limit (ppb)
Fe	DRC	54	Sc	Ammonia, 0.7	0.65	0.07
Al	DRC	27	Mg	Oxygen, 0.8	0.7	0.12
Zn	DRC	66	Sc	Oxygen, 0.9	0.7	0.06
Ti	DRC	46	Sc	Ammonia, 0.8	0.7	0.09
Ce	Standard	140	Sc	-	-	0.08
Ag	Standard	108	In	-	-	0.01

Table S2: Transport efficiencies for different metal NPs

NPs	Hydrodynamic diameter (nm)	Polydispersivity Index (PDI)	ε
TiO_2	151 ± 10	0.224 ± 0.015	0.75 ± 0.03
CeO_2	171 ± 12	0.196 ± 0.035	0.86 ± 0.05
ZnO	255 ± 23	0.543 ± 0.052	0.53 ± 0.09
Al_2O_3	251 ± 35	0.164 ±0.026	0.36 ± 0.15
	853 ± 25	0.343 ± 0.034	0.19 ± 0.10
Ag	100 ± 3	0.156 ± 0.026	0.97 ± 0.01

the transport efficiency. Furthermore, surface coating will likely affect the surface interactions and deposition of NPs onto the tubing and nebulizer chamber surfaces during the voyage into the plasma. If NPs tend to deposit on the rubber tubes or the glass or quartz surfaces of nebulizer chamber, the transport efficiency may be reduced. These potential factors from surface coating or adhesive characteristics of NPs are worth future investigations.

Conclusion

This study demonstrated that the transport efficiency did not vary with particle sizes of 25-120 nm and concentrations of 10-70 μg/L for monodisperse suspension of hematite NPs in the SP-ICP-MS analysis. However, the presence of dissolved ferric species substantially reduced the transport efficiency of hematite NPs. Moreover, polydisperse suspensions such as ZnO and Al_2O_3 NPs had significantly lower transport efficiencies than monodisperse suspension of NPs (e.g., AgNPs). Higher degree of aggregation of NPs in water dispersion likely reduced transport efficiencies during the particle nebulization and voyage into the plasma and thus affect the measurement accuracy of SP-ICP-MS. The results obtained from this study would lay groundwork toward a better framework of SP-ICP-MS analysis for NPs in water samples.

Acknowledgments

This study was partially supported by the Research Startup Fund at NJIT and National Science Foundation Grant CBET-1235166.

Supporting Information

Supplementary/ Supporting information for the system calibration and method optimization mentioned within the text are provided.

References

1. GAO (2010) Report to the Chairman, Committee on Environment and Public Works, U.S. Senate.
2. Djurisic AB, Leung YH, Ng AM, Xu XY, Lee PK, et al. (2015) Toxicity of metal oxide nanoparticles: mechanisms, characterization, and avoiding experimental artefacts. Small 11: 26-44.
3. Klaine SJ, Alvarez PJ, Batley GE, Fernandes TF, Handy RD, et al. (2008) Nanomaterials in the environment: behavior, fate, bioavailability, and effects. Environ Toxicol Chem 27: 1825-1851.
4. Chow JC, Watson JG, Savage N, Solomon CJ, Cheng YS, et al. (2005) Nanoparticles and the environment. J Air Waste Manag Assoc 55: 1411-1417.
5. Roco MC (2005) Environmentally responsible development of nanotechnology. Environ Sci Technol 39: 106A-112A.
6. Epstein HA (2011) Nanotechnology in cosmetic products. Skinmed 9: 109-110.
7. Kumar R, Anandan S, Hembram K, Rao TN (2014) Efficient ZnO-based visible-light-driven photocatalyst for antibacterial applications. ACS Appl Mater Interfaces 6: 13138-13148.
8. Ng YH, Leung YH, Liu FZ, Ng AMC, Gao MH, et al. (2013) Antibacterial activity of ZnO nanoparticles under ambient illumination – the effect of nanoparticle properties. Thin Solid Films 542: 368-372.
9. Babu VJ, Kumar MK, Nair AS, Kheng TL, Allakhverdiev SI, et al. (2012) Visible Light Photocatalytic Water Splitting for Hydrogen Production from N-TiO2 Rice Grain Shaped Electrospun Nanostructures. Int J Hydrogen Energ 37: 8897-8904.
10. Kozlova EA, Korobkina TP, Vorontsov AV (2009) Overall Water Splitting over Pt/TiO2 catalyst with Ce3+/Ce4+ Shuttle Charge Transfer System. Int J Hydrogen Energ 34: 138-146.
11. Chen C, Ma W, Zhao J (2010) Semiconductor-mediated photodegradation of pollutants under visible-light irradiation. Chem Soc Rev 39: 4206-4219.
12. Kubacka A, Fernández-García M, Colón G (2012) Advanced nanoarchitectures for solar photocatalytic applications. Chem Rev 112: 1555-1614.
13. Zhu X, Chang Y, Chen Y (2010) Toxicity and bioaccumulation of TiO2 nanoparticle aggregates in Daphnia magna. Chemosphere 78: 209-215.
14. Schwegmann H, Feitz AJ, Frimmel FH (2010) Influence of the zeta potential on the sorption and toxicity of iron oxide nanoparticles on S. cerevisiae and E. coli. J Colloid Interface Sci 347: 43-48.
15. Wong-Ekkabut J, Baoukina S, Triampo W, Tang IM, Tieleman DP, et al. (2008) Computer simulation study of fullerene translocation through lipid membranes. Nat Nanotechnol 3: 363-368.
16. Geiser M, Rothen-Rutishauser B, Kapp N, Schurch S, Kreyling W, et al. (2005) Ultrafine Particles cross Cellular Membranes by Nonphagocytic Mechanisms in Lungs and in Cultured Cells. Environ Health Perspect 113: 1555-1560.
17. Zhang W, Hughes J, Chen Y (2012) Impacts of hematite nanoparticle exposure on biomechanical, adhesive, and surface electrical properties of Escherichia coli cells. Appl Environ Microbiol 78: 3905-3915.
18. Trouiller B, Reliene R, Westbrook A, Solaimani P, Schiestl RH (2009) Titanium dioxide nanoparticles induce DNA damage and genetic instability in vivo in mice. Cancer Res 69: 8784-8789.
19. Bradford A, Handy RD, Readman JW, Atfield A, Mühling M (2009) Impact of silver nanoparticle contamination on the genetic diversity of natural bacterial assemblages in estuarine sediments. Environ Sci Technol 43: 4530-4536.
20. Zhang W, Yao Y, Chen Y (2011) Imaging and Quantifying the Morphology and Nanoelectrical Properties of Quantum Dot Nanoparticles Interacting with DNA. J Phys Chem C 115: 599–606.
21. Brunner TJ, Wick P, Manser P, Spohn P, Grass RN, et al. (2006) In vitro cytotoxicity of oxide nanoparticles: comparison to asbestos, silica, and the effect of particle solubility. Environ Sci Technol 40: 4374-4381.
22. Gupta AK, Gupta M (2005) Cytotoxicity suppression and cellular uptake enhancement of surface modified magnetic nanoparticles. Biomaterials 26: 1565-1573.
23. Hussain SM, Hess KL, Gearhart JM, Geiss KT, Schlager JJ (2005) In vitro toxicity of nanoparticles in BRL 3A rat liver cells. Toxicol In Vitro 19: 975-983.

Citation: Zhang W, Yao Y (2015) Influences of Primary Particle Size, Concentration, Ionic Species, and Aggregation States on Transport Efficiency in Single Particle-Inductively Coupled Plasma-Mass Spectrometry Analysis of Metal-Based Nanoparticles. Int J Nanoparticles Nanotech 1:004

24. Brayner R, Ferrari-Iliou R, Brivois N, Djediat S, Benedetti MF, et al. (2006) Toxicological impact studies based on Escherichia coli bacteria in ultrafine ZnO nanoparticles colloidal medium. Nano Lett 6: 866-870.

25. Huang Z, Zheng X, Yan D, Yin G, Liao X, et al. (2008) Toxicological effect of ZnO nanoparticles based on bacteria. Langmuir 24: 4140-4144.

26. Baun A, Hartmann NB, Grieger K, Kusk KO (2008) Ecotoxicity of engineered nanoparticles to aquatic invertebrates: a brief review and recommendations for future toxicity testing. Ecotoxicology 17: 387-395.

27. Zhu X, Zhu L, Li Y, Duan Z, Chen W, et al. (2007) Developmental Toxicity in Zebrafish (Danio rerio) Embryos after Exposure to Manufactured Nanomaterials: Buckminsterfullerene Aggregates (nC60) and Fullerol. Environ Toxicol Chem 26: 976-979.

28. Zhu X, Wang J, Zhang X, Chang Y, Chen Y (2009) The impact of ZnO nanoparticle aggregates on the embryonic development of zebrafish (Danio rerio). Nanotechnology 20: 195103.

29. Zhu X, Zhu L, Chen Y, Tian S (2009) Acute Toxicities of Six Manufactured Nanomaterial Suspensions to Daphnia magna. Journal of Nanoparticle Research 11: 67-75.

30. Kim IS, Baek M, Choi SJ (2010) Comparative cytotoxicity of Al2O3, CeO2, TiO2 and ZnO nanoparticles to human lung cells. J Nanosci Nanotechnol 10: 3453-3458.

31. Rothen-Rutishauser BM, Schürch S, Haenni B, Kapp N, Gehr P (2006) Interaction of fine particles and nanoparticles with red blood cells visualized with advanced microscopic techniques. Environ Sci Technol 40: 4353-4359.

32. Zhang W, Kalive M, Capco DG, Chen Y (2010) Adsorption of hematite nanoparticles onto Caco-2 cells and the cellular impairments: effect of particle size. Nanotechnology 21: 355103.

33. Theng BKG, Yuan GD (2008) Nanoparticles in the Soil Environment. Elements 4: 395-399.

34. Simonet BM, Valcárcel M (2009) Monitoring nanoparticles in the environment. Anal Bioanal Chem 393: 17-21.

35. Laborda F, Jiménez-Lamana J, Bolea E, Castillo JR (2011) Selective Identification, Characterization and Determination of Dissolved Silver (I) and Silver Nanoparticles based on Single Particle Detection by Inductively Coupled Plasma Mass Spectrometry. Journal of Analytical Atomic Spectrometry 26: 1362-1371.

36. Mitrano DM, Barber A, Bednar A, Westerhoff P, Higgins CP, et al. (2012) Silver Nanoparticle Characterization using Single Particle ICP-MS (SP-ICP-MS) and Asymmetrical Flow Field Flow Fractionation ICP-MS (AF4-ICP-MS). Journal of Analytical Atomic Spectrometry 27: 1131-1142.

37. Mitrano DM, Ranville JF, Bednar A, Kazor K, Hering AS, et al. (2014) Tracking Dissolution of Silver Nanoparticles at Environmentally Relevant Concentrations in Laboratory, Natural, and Processed waters using Single Particle ICP-MS (spICP-MS). Environmental Science: Nano 1: 248-259.

38. Allabashi R, Stach W, de la Escosura-Muñiz A, Liste-Calleja L, Merkoçi A (2009) ICP-MS: a Powerful Technique for Quantitative Determination of Gold Nanoparticles without Previous Dissolving. Journal of Nanoparticle Research 11: 2003-2011.

39. Tuoriniemi J, Cornelis G, Hassellov M (2014) Improving the Accuracy of Single Particle ICPMS for Measurement of Size Distributions and Number Concentrations of Nanoparticles by Determining Analyte Partitioning during Nebulisation. Journal of Analytical Atomic Spectrometry 29: 743-752.

40. Santos MC, Nóbrega JA (2006) Slurry Nebulization in Plasmas for Analysis of Inorganic Materials. Applied Spectroscopy Reviews 41: 427-448.

41. Pace HE, Rogers NJ, Jarolimek C, Coleman VA, Higgins CP, et al. (2011) Determining Transport Efficiency for the Purpose of Counting and Sizing Nanoparticles via Single Particle Inductively Coupled Plasma Mass Spectrometry. Analytical Chemistry 83: 9361-9369.

42. Ebdon L, Collier A (1988) Particle Size Effects on Kaolin Slurry Analysis by Inductively Coupled Plasma-Atomic Emission Spectrometry. Spectrochimica Acta Part B: Atomic Spectroscopy 43: 355-369.

43. Van Borm WA, Broekaert JA, Klockenkämper R, Tschopel P, Freddy A (1991) Aerosol Sizing and Transport Studies with Slurry Nebulization in Inductively Coupled Plasma Spectrometry. Spectrochimica Acta Part B: Atomic Spectroscopy 46: 1033-1049.

44. Mochizuki T, Sakashita A, Iwata H, Ishibashi Y, Gunji N (1991) Application of Slurry Nebulization to Trace Elemental Analysis of Some Biological Samples by Inductively Coupled Plasma Mass Spectrometry. Fresenius' journal of analytical chemistry 339: 889-894.

45. Gottschalk F, Sonderer T, Scholz RW, Nowack B (2010) Possibilities and limitations of modeling environmental exposure to engineered nanomaterials by probabilistic material flow analysis. Environ Toxicol Chem 29: 1036-1048.

46. Gottschalk F, Sonderer T, Scholz RW, Nowack B (2009) Modeled environmental concentrations of engineered nanomaterials (TiO(2), ZnO, Ag, CNT, Fullerenes) for different regions. Environ Sci Technol 43: 9216-9222.

47. Horie M, Nishio K, Fujita K, Endoh S, Miyauchi A, et al. (2009) Protein adsorption of ultrafine metal oxide and its influence on cytotoxicity toward cultured cells. Chem Res Toxicol 22: 543-553.

48. Fabian E, Landsiedel R, Ma-Hock L, Wiench K, Wohlleben W, et al. (2008) Tissue distribution and toxicity of intravenously administered titanium dioxide nanoparticles in rats. Arch Toxicol 82: 151-157.

49. Senzui M, Tamura T, Miura K, Ikarashi Y, Watanabe Y, et al. (2010) Study on penetration of titanium dioxide (TiO(2)) nanoparticles into intact and damaged skin in vitro. J Toxicol Sci 35: 107-113.

50. Van Hoecke K, Quik JT, Mankiewicz-Boczek J, De Schamphelaere KA, Elsaesser A, et al. (2009) Fate and effects of CeO2 nanoparticles in aquatic ecotoxicity tests. Environ Sci Technol 43: 4537-4546.

51. Zhang W, Zhang X (2015) Adsorption of MS2 on oxide nanoparticles affects chlorine disinfection and solar inactivation. Water Res 69: 59-67.

52. Li Y, Niu J, Zhang W, Zhang L, Shang, E (2014) Influence of Aqueous Media on the ROS-Mediated Toxicity of ZnO Nanoparticles toward Green Fluorescent Protein-Expressing Escherichia coli under UV-365 Irradiation. Langmuir 30: 2852-2862.

53. Zhang W, Li Y, Niu J, Chen Y (2013) Photogeneration of reactive oxygen species on uncoated silver, gold, nickel, and silicon nanoparticles and their antibacterial effects. Langmuir 29: 4647-4651.

54. Li Y, Zhang W, Niu J, Chen Y (2012) Mechanism of photogenerated reactive oxygen species and correlation with the antibacterial properties of engineered metal-oxide nanoparticles. ACS Nano 6: 5164-5173.

55. Li Y, Zhang W, Li K, Yao Y, Niu J, et al. (2012) Oxidative dissolution of polymer-coated CdSe/ZnS quantum dots under UV irradiation: mechanisms and kinetics. Environ Pollut 164: 259-266.

56. Li K, Chen Y, Zhang W, Pu Z, Jiang L, et al. (2012) Surface interactions affect the toxicity of engineered metal oxide nanoparticles toward Paramecium. Chem Res Toxicol 25: 1675-1681.

57. Zhang W, Yao Y, Sullivan N, Chen Y (2011) Modeling the primary size effects of citrate-coated silver nanoparticles on their ion release kinetics. Environ Sci Technol 45: 4422-4428.

58. Zhang W, Yao Y, Li K, Huang Y, Chen Y (2011) Influence of dissolved oxygen on aggregation kinetics of citrate-coated silver nanoparticles. Environ Pollut 159: 3757-3762.

59. Zhang W, Rittmann B, Chen Y (2011) Size effects on adsorption of hematite nanoparticles on E. coli cells. Environ Sci Technol 45: 2172-2178.

60. Zhang W (2011) Characterization, Imaging, and Quantifing the Environmental Behaviro and Biological Interactions of Metal-based Nanoparticles.

61. Boxall ABA, Chaudhry Q, Sinclair C, Jones A, Aitken R (2007) Current and Future Predicted Environmental Exposure to Engineered Nanoparticles. Central Science Laboratory, UK.

62. Zachariadis GA, Sahanidou E (2009) Multi-element method for determination of trace elements in sunscreens by ICP-AES. J Pharm Biomed Anal 50: 342-348.

Citation: Zhang W, Yao Y (2015) Influences of Primary Particle Size, Concentration, Ionic Species, and Aggregation States on Transport Efficiency in Single Particle-Inductively Coupled Plasma-Mass Spectrometry Analysis of Metal-Based Nanoparticles. Int J Nanoparticles Nanotech 1:004